**Wind and Structures**, *Vol. 30, No. 3 (2020) 261-273*
DOI: https://doi.org/10.12989/was.2020.30.3.261


# Modeling and experimental comparative analysis on the performance of small-scale wind turbines

Ehab Basta[1], Mehdi Ghommem[*1] and Lotfi Romdhane[1] and Abdessattar Abdelkefi[2]

*[1]Department of Mechanical Engineering, American University of Sharjah, Sharjah 26666, UAE*
*[2]Department of Mechanical and Aerospace Engineering, New Mexico State University, Las Cruces, NM 88003, USA*

*(Received April 2, 2019, Revised December 21, 2019, Accepted January 4, 2020)*

**Abstract**. This paper deals with the design, wind tunnel testing, and performance analysis of small wind turbines targeting low-power applications. Three different small-size blade designs in terms of size, shape, and twisting angle are considered and tested. We conduct wind tunnel tests while measuring the angular speed of the rotating blades, the generated voltage, and the current under varying resistive loading and air flow conditions. An electromechanical model is also used to predict the measured voltage and power and verify their consistency and repeatability. The measurements are found in qualitative agreement with those reported in previously-published experimental works. We present a novel methodology to estimate the mechanical torque applied to the wind turbine without the deployment of a torque measuring device. This method can be used to determine the power coefficient at a given air speed, which constitutes an important performance indicator of wind turbines. The wind tunnel tests revealed the capability of the developed wind turbines to deliver more than 1225 mW when subject to an air flow with a speed of 7 m/s. The power coefficient is found ranging between 26% and 32%. This demonstrates the aerodynamic capability of the designed blades to extract power from the wind.

**Keywords:** miniature wind turbine; wind tunnel testing; performance analysis; energy harvesting; electromechanical model

## 1. Introduction

Several energy harvesting technologies including piezoelectric, electrostatic, magnetostrictive, photovoltaic, and thermoelectric have been introduced and utilized in the past decade (Syta *et al*. 2015, Erturk and Inman 2011, Castagnetti and Radi 2018). These energy harvesters can efficiently convert any wasted mechanical or heat energy to electrical energy and hence operate various low-power consumption devices, such as cell phones, cameras, pacemakers, wireless sensors, structural health monitoring sensors, and others (Ottman *et al*. 2002, Sodano *et al*. 2005). However, these energy harvesting transductions have issues. Indeed, for thermal-based energy harvesters, the wasted heat/solar energy cannot be continuously transformed to electrical energy due to the absence of the thermal source at nights and in shaded areas. Concerning the vibratory-based energy harvesters, most of them have issues in the level of the harvested power and complications in the design of the system depending on the environmental conditions and structural fatigue (Ottman *et al*. 2002, Sodano *et al*. 2005, Zhou *et al*. 2018). One of the solutions can be the wind turbine technology which is well established for large scale systems. Wind power currently provides about 3.5% of global electricity demand, and it is expected that the wind energy share could reach up to 12% by 2020. The global wind power capacity has recently exhibited an increase of over 133.5%. Over the last few decades, mid-scale wind turbines have gained attention several researchers and companies (Bukala *et al*. 2016, Tarhan and Yilmaz 2019, Carta *et al*. 2015, Shah *et al*. 2014, Morshed *et al*. 2013, Roy and Saha 2015). These systems produce power in the order of few kilowatts and can serve as complement to power buildings in urban environments (Bukala *et al*. 2016, Tarhan and Yilmaz 2019). For small-scale designs which can be an attractive alternative to operate low-power consumption devices (Xu *et al*. 2014), only few numerical and experimental studies have been conducted to examine the performance and operating conditions of these systems (Kishore *et al*. 2013, Kishore and Priya 2013, Xu *et al*. 2013, Zakariya *et al*. 2015, Howey *et al*. 2011, Xu *et al*. 2014, Priya *et al*. 2005, Hirahara *et al*. 2005, Costa Rocha *et al*. 2018, Du *et al*. 2018).

The small-scale wind turbine systems can be deployed to power portable electronics, in isolated or abandoned areas (Perez *et al*. 2016), home security systems, and wireless sensing systems implemented in confined and inaccessible spaces such as structural health monitoring system of high-rise buildings and bridges (Park *et al*. 2012). In these infrastructures, wiring and replacing chemical batteries require perpetual and careful maintenance (De Broe *et al*. 1999). Therefore, this type of wind turbines constitutes a good substitute of chemical batteries, given their limited energy density and short life-span, which present a critical issue in providing reliable and continuous power supply. However, it should be noted that the wind turbine efficiency can reduce from 40%, which is attainable for large-scale systems (rotor diameter > 5 m) to less than

*Corresponding author, Ph.D.
E-mail: mghommem@aus.edu


http://www.techno-press.com/journals/was&subpage=7 ISSN: 1226-6116 (Print), 1598-6225 (Online)

10% when the size of the rotor tip diameter is in the order of few centimeters (Kishore *et al*. 2013, Kishore and Priya 2013, Xu *et al*. 2013, Zakariya *et al*. 2015, Xu *et al*. 2014). The significant reduction in the efficiency is mainly associated to the drastic drop in the lift-to-drag ratio resulting from the decrease in the Reynolds number, frictional losses of the mechanical part (bearings and gear system), and potential electromagnetic interferences of small generators.

Several numerical and experimental studies have been recently conducted to analyze the performance of small wind turbines. Xu *et al*. (2013) demonstrated the capability of a small horizontal axis wind turbine with a tip diameter of 7.6 cm to produce 110 mW and reach an overall efficiency of 7.6% at wind speed of 8 m/s. They also developed an electromechanical model to predict the output voltage and power of the wind turbine for varying load resistances. The modeling results are found in good agreement with their experimental counterparts showing the predictive capability of the proposed model and its possible use for optimization and design purposes. Kishore *et al*. (2013) presented details on the design, construction, and characterization of a small-scale wind energy portable turbine, namely SWEPT, operating at low wind speeds (below 5 m/s). They conducted computational fluid dynamics (CFD) analysis to design a diffuser, which was implemented on the wind turbine to enhance its performance. The incorporation of the diffuser is observed to increase the electrical power generation by a factor of 1.4 to 1.6. Kishore and Priya 2013 carried out a combined theoretical and experimental study on a small wind turbine with a tip diameter of 40 cm. The wind tunnel experiments showed that the developed wind turbine can produce an electrical power of 2.2 W at a wind speed of 5.5 m/s. They presented an alternative method for the computation of the mechanical power without the direct measurements of the shaft torque generated by the wind turbine. The proposed method is based on the calculation of the time rate of the change of the angular speed, measured using an optical tachometer, and the moment of inertia of the wind turbine rotor about the axis of rotation estimated using a CAD software. The wind turbine reached a power coefficient of 32% and overall efficiency of 21% at 4 m/s. Park *et al*. (2012) presented a feasibility study of small wind turbines to generate sufficient electricity to power wireless sensors used for structural health monitoring of a cable-stayed bridge. The characteristics of the wind environment at the bridge site has been first investigated to identify the dominant wind speed and direction. Then, they conducted a performance analysis of different wind turbine designs using the wind tunnel. They found that exposing the wind turbine at a wind speed of 7 m/s (when operating at optimal loading conditions) for a duration of 19.8 minutes is sufficient to produce the required power of the wireless sensors mounted on the bridge for one day. Zakaria *et al*. (2015) conducted an experimental study of a swirl-type micro-wind turbine with a rotor tip diameter of 2.6 cm. The maximum output power generated by the micro wind turbine is found equal to 2.72 mW and it is obtained at a wind speed of 6.5 m/s when setting the load resistance at 330 Ω leading to an overall efficiency of 3.24%. They have also tested the impact of the incident flow direction on the wind turbine performance. They found that the power generation is not affected as long as the yaw angle remains within $\pm 10^o$.

In this work, we design and implement three miniature horizontal axis wind turbines with varying characteristics in terms of rotor size and blade geometry. We conduct wind tunnel tests to investigate their performance when exposed to different air flow and loading conditions. The experimental measurements include the angular speed of the rotating blades, the output voltage, and the current. The measured output voltage and power under different operating conditions are found in good agreement with those obtained from an electromechanical model. These measurements are also qualitatively consistent with those reported in previously-published experimental works. The present study provides an alternative method to estimate the mechanical power by combining the use of an electromechanical model and the aforementioned experimental measurements without the deployment of a torque measuring device. Such method is helpful to determine the power coefficient at a given air speed, which constitutes an important parameter to characterize the performance of wind turbines. The estimated power coefficient of the tested wind turbines is found in the range of 26% - 32% while the efficiency of the gear-generator system is observed ranging between 6.5% and 11.5%. These results indicate the aerodynamic capabilities of the used blades to convert efficiently the available wind to mechanical energy. However, the generator shows low performance in generating electrical power and then results in low efficiency values. The rest of the paper is organized as follows: Section 2 presents the specifications of the three designs of the wind turbines. The experimental set-up and procedure are described in Section 3. The experimental and numerical results obtained from the wind tunnel tests and the electromechanical model, respectively, are compared and discussed in Section 4. Details on the proposed method to determine the mechanical power of the rotor are also presented in Section 4. The main outcomes of the present study are summarized in Section 5.

## 2. Design and development of the small-scale wind turbine

The performance of a small wind turbine depends mainly on the blade design, airfoil section, twist angle pitch angle, and variation of the chord length along the spanwise direction, transmission system connecting the rotor of the wind turbine to the generator, electrical circuit components, and generator. The assessment of the performance of wind turbines is made through the estimation of two main parameters, namely, the power coefficient $C_p$ and the overall efficiency $\eta$ (Kishore *et al.* 2013, Kishore and Priya 2013, Xu *et al.* 2013, Zakariya *et al.* 2015, Xu *et al.* 2014). $C_p$ is defined as the ratio of the mechanical power over the available wind power; that is,

$$C_p = \frac{P_{mech}}{(1/2\rho A U^3)} = \frac{T\omega}{(1/2\rho A U^3)} \tag{1}$$

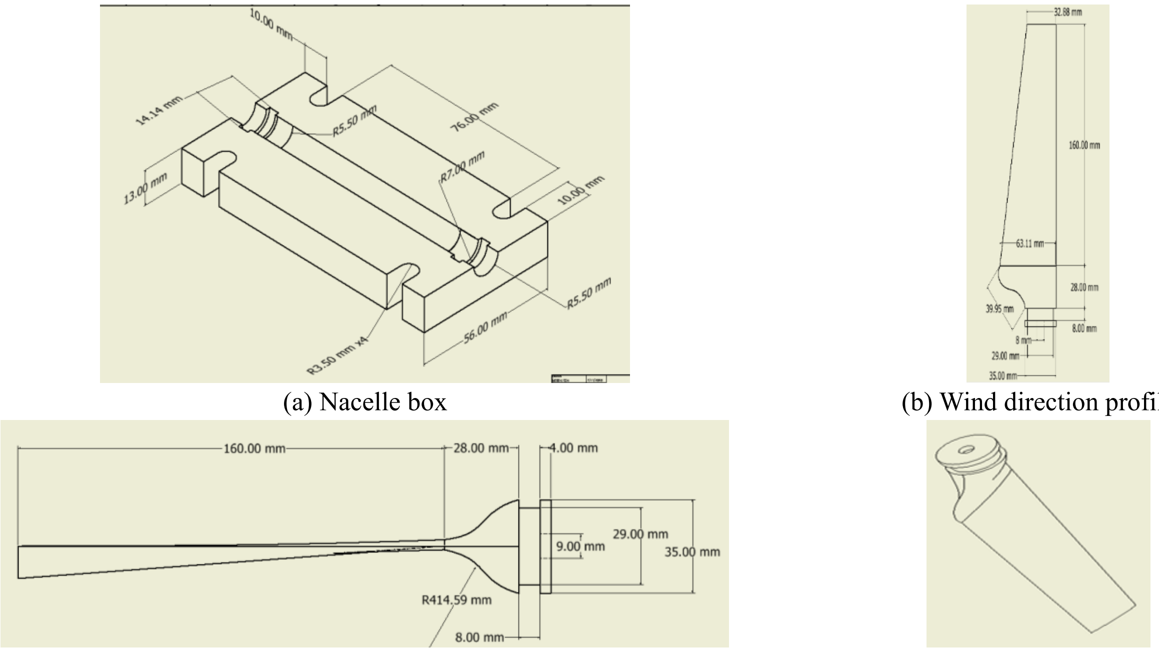


(a) Nacelle box (b) Wind direction profile

(c) Blade (side view) (d) Blade (isometric view)

Fig. 1 Blade and nacelle design characteristics (WT3)

Table 1 Wind turbines dimensions and characteristics.

| | WT1 | WT2 | WT3 |
|---|---|---|---|
| Rotor axis | | Horizontal | |
| Rotor diameter $D$ | 68 cm | 48 cm | 48 cm |
| Airfoil | | NACA 0012 | |
| Blade length (root to tip) | 30 cm | 20 cm | 20 cm |
| Blade chord length (tip) | 3.7 cm | 2.9 cm | 3.288 cm |
| Pitch angle of the blades | 25° | 30° | 30° |
| Twist angle (hub) | 7° (max) | 0° | 0° |
| Twist angle (tip) | 0° | 10° (max) | 20° (max) |
| Number of blades | | 3 | |
| Gear ratio $n$ | | 8:1 | |
| Generator type | | Permanent magnet DC motor | |
| Electromechanical coefficient of the generator $K$ | | 17.36 $10^{-3}$ V/rad/s | |
| Internal resistance $R$ | | 60 Ω | |
| Cut-in wind speed | 2.3 m/s | 3.8 m/s | 2.8 m/s |

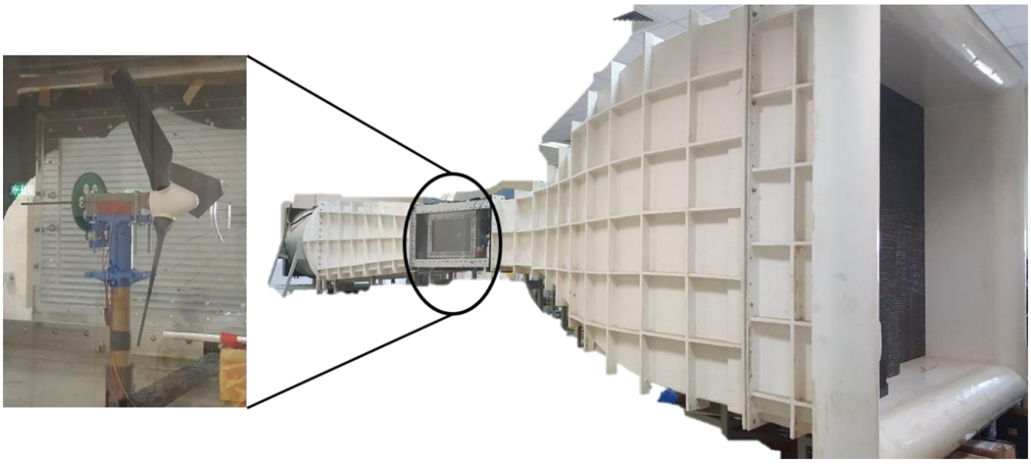

Fig. 2 Small-scale wind turbine mounted in the wind tunnel.

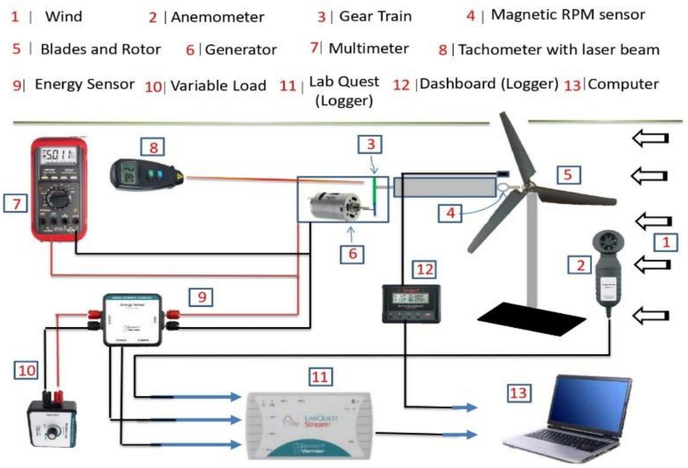


Fig. 3 Wind tunnel experimental set-up.

where $\rho$ denotes the air density, $A$ is the area swept by the blades of the wind turbine, $U$ represents the air speed, $T$ is the torque, and $\omega$ is the angular speed of the rotor. The overall efficiency $\eta$ is given by the ratio of the generated electrical power over the available wind power, expressed as

$$\eta = \frac{P_{elec}}{(1/2\rho AU^3)} = \frac{VI}{(1/2\rho AU^3)} \quad (2)$$

where $V$ and $I$ are the generated voltage and current, respectively. A resistive load needs to be applied to the generator to produce current. In the present study, the performance analysis of the wind turbines is based on measuring the generated electrical power and the overall efficiency. We also develop an alternative method to estimate the power coefficient without performing direct measurements of the torque applied on the rotor of the wind turbine as will be described in the subsequent section. The main design requirements of the wind turbines are to be portable, have a small size (rotor diameter is between 10 cm and 100 cm) and light weight, with a capability to operate in low air speed environments and generate electrical power in the order of hundreds of mW as needed to function wireless sensors and small electronic devices (Park *et al.* 2012, Zakaria *et al.* 2015). We also target to develop wind turbines with reasonable power coefficient and overall efficiency when compared to those reported in the literature (Kishore *et al.* 2013, Kishore and Priya 2013, Xu *et al.* 2013, Zakariya *et al.* 2015, Howey *et al.* 2011, Xu *et al.* 2014, Priya *et al.* 2005) and have structural strength to resist mechanical shocks and abrupt acceleration of the air flow.

The initial design consisted of commercially available off-the-shelf blades to construct the small wind turbine (ScienceKit 2018). Hereafter, we refer to this turbine as WT1. The rotating blades with a length of 30 cm are made of plastic with NACA 0012 airfoil section. The twist angle is an important parameter that affects the power coefficient of a wind turbine (Kishore *et al.* 2013, Kishore and Priya 2013, Xu *et al.* 2013, Zakariya *et al.* 2015). The power coefficient dictates the aerodynamic capability of the wind turbine to extract power from the available kinetic power from the airflow. The blades of the wind turbine WT1 are slightly twisted from the hub to the tip. We consider two other blade designs with smaller size to enable better portability. These blades are linearly twisted by 10$^o$ and 20$^o$ from the tip to the hub. We denote by WT2 and WT3 the wind turbines equipped with the blades twisted by 10$^o$ and 20$^o$, respectively. NACA 0012 airfoil section is selected for the blade design given its suitability for operation at low Reynolds number (Kishore *et al.* 2013, Kishore and Priya 2013) and to avoid potential defects when 3D printing cambered blades. Further details on the geometry of the blade design are shown in Fig. 1. All dimensions are reported in mm. We note that the shape of the blades considered in the present experimental study resembles that of its large counterpart as shown in Fig. 1(b). Twisting the blades from the hub is observed to initiate the rotational motion of the blades at lower air speeds. The cut-in speed is found equal to 2.3 m/s, 3.8 m/s, and 2.8 m/s for the wind turbines WT1, WT2, and WT3, respectively. Different trials were performed at various pitch angles and it was observed that the highest power generation is obtained when setting the pitch angle at 25$^o$-30$^o$.

The nacelle is considered the same for all tested wind turbines. It is designed and 3D printed to hold the shaft relating the rotor hub and the gear train connected to the generator. Fig. 1(a) displays the detailed CAD model of the lower component of the nacelle box. Bearings are placed inside grooves and slots for screws are drilled to enable the stability of the set-up when subject to fluctuating incident flow conditions. The two bearings are used to smoothen the rotation of the blades and dampen the vibrations of the wind turbine at when operating at high air speeds. The shaft was fabricated to connect between the rotor hub and the driving gear, which is attached to the generator. The ratio of the gear system is selected to 8:1 in order to speed up the rotational motion of the generator shaft. A permanent magnet DC motor is used as the generator to produce power from the airflow. Table 1 presents the design characteristics of the tested wind turbines. Each includes three blades, a rotor, nacelle, gear system and permanent magnet DC motor to generate power from the rotational motion induced by the wind.

## 3. Experimental setup

Wind tunnel tests were carried out in the aeronautics lab at the American University of Sharjah (AUS) (shown in Fig. 2) to evaluate the performance of the developed wind turbines. The rotational motion of the blades is transmitted to the generator and amplified via the gear system. The produced current from the generator passes through a tunable resistive load to measure the power generation.

The wind tunnel is tapered, and the air flow is initiated from a fan that is forced to pass through a honeycomb structure to obtain a steady uniform air flow over the cross-sectional area at which the experiment is conducted. The dimensions of the cross section of the testing chamber are 72 cm and 90 cm (see Fig. 2). We vary the wind speed between 2 and 7 m/s in the present experimental study. We display in Fig. 3 a detailed schematic of the experimental setup with all devices and sensors used for the experimental study. We place an anemometer (ANM-BTA, Vernier, Inc.) about 5 cm in front of the rotating blades and connect it to a data logger (LabQuest, Vernier, Inc.) to monitor and record the air speed. The anemometer can measure wind speeds in the range of 0.5 to 30 m/s and it has a resolution of 0.012 m/s. We note that several measurements are taken at different locations within 5-10 cm upstream of the rotor away from the wind tunnel walls to avoid the side effects. Minor variations in the anemometer readings are observed. This indicates the insensitivity of the air speed measurements to the rotational motion of the blades at the considered plane. We use an energy sensor (VES-BTA, Vernier, Inc.), which is connected

directly to the generator to measure the output. We verify also these measurements by comparing them against those retrieved from a Voltmeter. The Vernier energy sensor has a resolution of 8 mV (voltage sensor) and 0.26 mA (current sensor). The anemometer and the energy sensor are connected to a data logger to acquire and process the data using a computer software (Logger Lite, Vernier, Inc.). We deploy a variable resistance box to obtain the experimental data when the electrical part of the wind turbine undergoes varying loading conditions. This resistance box allows for varying the resistance load within a range of 8-255 Ω. The performance of the small wind turbines is assessed for resistive load ranging from 10 to 200 Ω. The internal resistance is measured directly from an ohmmeter of the open-circuit configuration.

An RPM magnet sensor (Eagle Tree Systems) is mounted in the proximity of the rotor shaft to measure the angular velocity of the rotating blades. We place this sensor about 1-2 mm away from the magnet, which is tightly glued on the rotor shaft. The accurate measurement of the angular speed in the blades placed inside the testing chamber of the wind tunnel is crucial in our experimental study. Therefore, we verify and compare the angular speed obtained from three different RPM sensors. These are magnet, laser non-contact tachometer, and optical sensors. A calibrated laboratory set-up consisting of a controlled rotating shaft attached to a DC motor is deployed before mounting any of these sensors in the wind turbine. We vary the angular speed of the rotating shaft of the calibrated laboratory set-up by

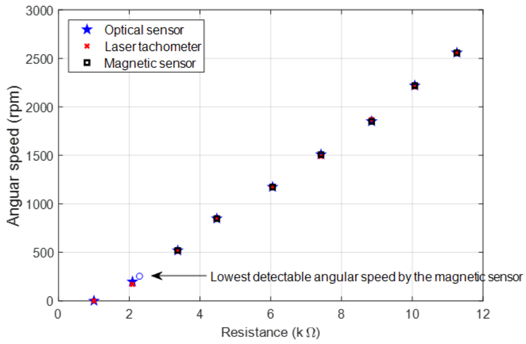


Fig. 4 Comparison of the acquired angular speeds from three different RPM sensors

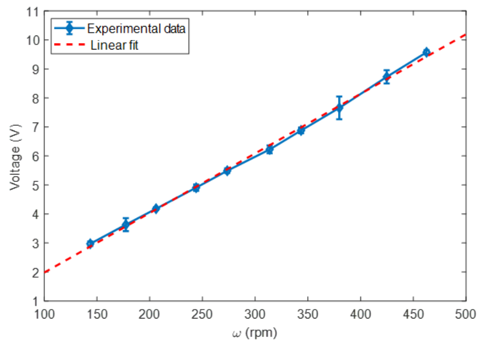


Fig. 5 Generated voltage as function of the angular speed of the turbine (open-circuit configuration)

altering the load resistance. The magnetic RPM sensor is based on the Hall effect to measure the angular speed of a rotating body. It should be noted that this type of sensor is very sensitive to the mounting of the magnet on the rotating shaft. A reflective tape is also placed on the shaft and a non-contact digital laser tachometer (RPM meter DT2234C) is used to enable further verification of the angular speed measurements. The laser beam of the tachometer needs to be carefully exposed to the reflective tape to indicate a constant value. We note that the aforementioned set-up includes also a calibrated optical sensor. We show in Fig. 4 the experimental measurements obtained from the three RPM sensors. All the acquired data are in good agreement indicating the reliability of the selected sensors. In the subsequent study, we measure the angular speed from both the laser tachometer and the magnetic RPM sensor when varying the air speed and the load resistance. We repeat the experiments four times while monitoring and recording the air speed in the testing chamber of the wind tunnel, the angular speed of the rotor shaft, the voltage, and the current generated by the wind turbine for different load resistance values and then we compute the mean and standard deviation values to verify the repeatability and consistency of the measurements.

To characterize the used off-the-shelf generator, we first measure the electromechanical coefficient of the DC generator. This parameter will be used in the performance predictive model to be presented in the subsequent section. To do so, we record the values of the generated voltage of the open circuit in absence of any resistance load when varying the angular speed of the wind turbine rotor $\omega$ by changing the wind tunnel air speed from 2.5 m/s to 7 m/s. The corresponding results are displayed in Fig. 5. As expected, a linear trend is obtained. The value of the electromechanical coefficient is determined from the slope of the linear fitting. It is found equal to 2.17 $10^{-3}$ V/rad/s. To obtain the conversion coefficient relating the produced voltage from the generator to the angular speed of the generator shaft, we divide the aforementioned value by the gear ratio.

## 4. Experimental results and performance evaluation

We employ the experimental set-up described in the previous section to analyze the performance of the developed wind turbine under different operating conditions. We control the air speed of the wind tunnel and measure the angular speed of the rotating blades using the magnet RPM sensor and the air speed using the anemometer. We also vary the load resistance and measure the voltage, current, and electrical power generated by the wind turbine.

### *4.1 Electromechanical model*

We follow Xu *et al.* (2013) to develop an electromechanical model to predict the power generation of the wind turbines and estimate the mechanical power without the use of a torque sensor. Fig. 6 shows the coupled equivalent electrical circuit and the mechanical system.
The gear ratio is defined as follows

$$n = \frac{\omega_G}{\omega} = \frac{T}{T_m} \tag{3}$$

where $\omega$ denotes the angular velocity of the wind turbine, $\omega_G$ is the angular velocity of the generator, $T$ is the mechanical torque on the wind turbine shaft, and $T_m$ is the mechanical torque on the generator shaft. Following Kirchoff's voltage law (KVL), the output voltage $V$ is given by

$$V(t) = -Ri(t) - L\frac{di(t)}{dt} + e = R_L i(t) \tag{4}$$

where $R$ is the internal resistance of the generator, $i$ represents the current in the generator circuit, $L$ is the inductance of the generator, and $R_L$ is the electrical load resistance. $e$ denotes the induced voltage due to the rotational motion of the generator armature. It is expressed as

$$e = K\omega_G \tag{5}$$

Here, $K$ denotes the torque constant of the generator. The output voltage can be expressed then as follows

$$V(t) = -Ri(t) - L\frac{di(t)}{dt} + K\omega_G = R_L i(t) \tag{6}$$

Rewriting Eq. 6 in terms of the current, we obtain

$$i(t) = \frac{1}{R_L + R}\left(-L\frac{di(t)}{dt} + K\omega_G\right) \tag{7}$$

The effect of the induction on the small generator is minor and then the term $L$ in Eq. (7) is neglected. Therefore, the steady-state current and output voltage are expressed as

$$i = \frac{K\omega_G}{R_L + R} \tag{8}$$

$$V = \frac{R_L}{R_L + R}K\omega_G \tag{9}$$

The output power is given then by

$$P = V.i = \frac{R_L K^2 {\omega_G}^2}{(R_L + R)^2} = n^2\frac{R_L K^2 \omega^2}{(R_L + R)^2} \tag{10}$$

The governing equation of the mechanical part can be obtained by applying Newton's law; that is,

$$T_m - T_G - B\omega_G = \left(J_G + \frac{J_t}{n^2}\right)\frac{d\omega_G}{dt} \tag{11}$$

Here, $J_t$ is the moment of inertia of the turbine, $J_G$ denotes the moment of inertia of the generator, and $B$ is the damping constant (friction coefficient) of the bearings. $T_G$ represents the electro-magnetic torque on the generator shaft expressed in terms of the generated current as

$$T_G = Ki(t) \tag{12}$$

Using Eqs. (3), (8), (11) and (12), the drive torque of the wind turbine $T$ is derived as

$$T = n\left(\frac{K^2\omega_G}{R_L + R} + B\omega_G + \left(J_G + \frac{J_t}{n^2}\right)\frac{d\omega_G}{dt}\right) \tag{13}$$

Rewriting Eq. (13) in terms of the angular speed of the wind turbine, we obtain

$$T = \frac{(nK)^2\omega}{R_L + R} + n^2 B\omega + (n^2 J_G + J_t)\frac{d\omega}{dt} \tag{14}$$

At the steady state, the angular velocity remains constant. Therefore, the expression of the mechanical torque becomes

$$T = n^2\left(\frac{K^2}{R_L + R} + B\right)\omega \tag{15}$$

As shown in Eq. (15), for a given load resistance $R_L$, the ratio $T/\omega$ remains unchanged and then it can be considered as constant. Hence, using Eqs. 10 and 15, the electric output power can be expressed in terms of the mechanical torque as

$$P = \frac{T^2 R_L K^2}{n^2\left(K^2 + B(R_L + R)\right)^2} \tag{16}$$

For a given air speed $U$, the drive torque can be considered as a constant (Xu *et al.* 2013). Therefore, the optimal load resistance can be obtained by setting the derivative of the power with respect to the load resistance $\frac{\partial P}{\partial R_L}$ equal to zero. This leads to

$$R_L^{opt} = R + \frac{K^2}{B} \tag{17}$$

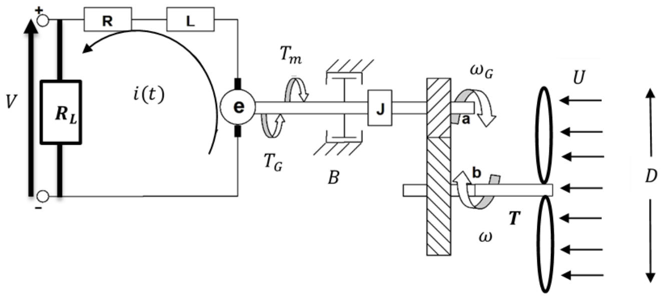


Fig. 6 Schematic of the equivalent electromechanical model of the wind turbine.

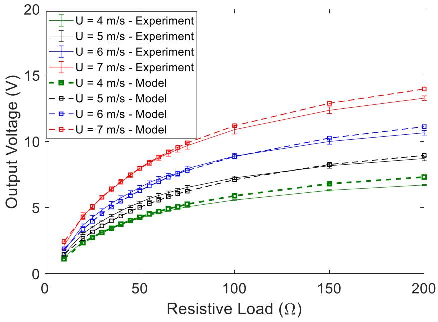


(a) WT1

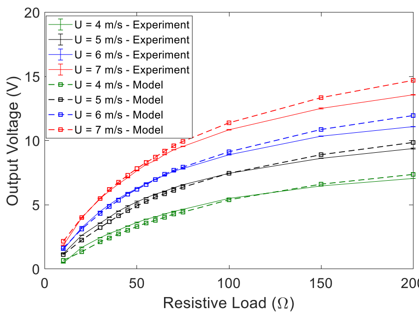


(b) WT2

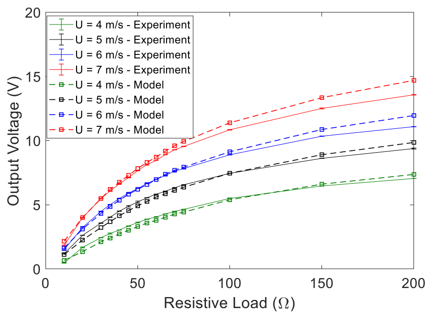


(c) WT3

Fig. 7 Generated voltage vs. the load resistance at varying air speed for different wind turbines: comparison between experimental (solid line) and numerical (dashed line) results.

and the corresponding maximum generated power is given by

$$P^{opt} = \frac{T^2K^2}{4n^2B(K^2+RB)} \tag{18}$$

Therefore, the torque can be obtained from Eq. 16

$$T = \sqrt{\frac{4n^2B(K^2+RB)\ \ P^{opt}}{K^2}} \tag{19}$$

Inspecting Eq. (18), we note that the optimum power is inversely proportional to the internal resistance of the generator. Therefore, a generator with smaller internal resistance $R$ yields a higher optimal power for a given wind speed.

The electromechanical model described above is used to verify the consistency of the experimental data acquired from the different tested wind turbines. A comparative study between the experimental and numerical results will be conducted in the subsequent subsection. We use also the electromechanical model to estimate the mechanical torque applied to the wind turbines at different operating conditions.

### *4.2 Electromechanical model*

We present the experimental measurements obtained for the three wind turbines under investigation. The goal is to assess their performance under varying operating conditions. Fig. 7 displays the variations of the measured output DC voltage of the generator with the load resistance for air speeds ranging from 4 to 7 m/s. The experimental results are obtained for the different wind turbines considered in the present study. We show also the numerical predictions of the output voltage as given by Eq. (9). Note that the value of the conversion coefficient $K$ is determined experimentally and found equal to 17.36 $10^{-3}$ V/rad/s. A

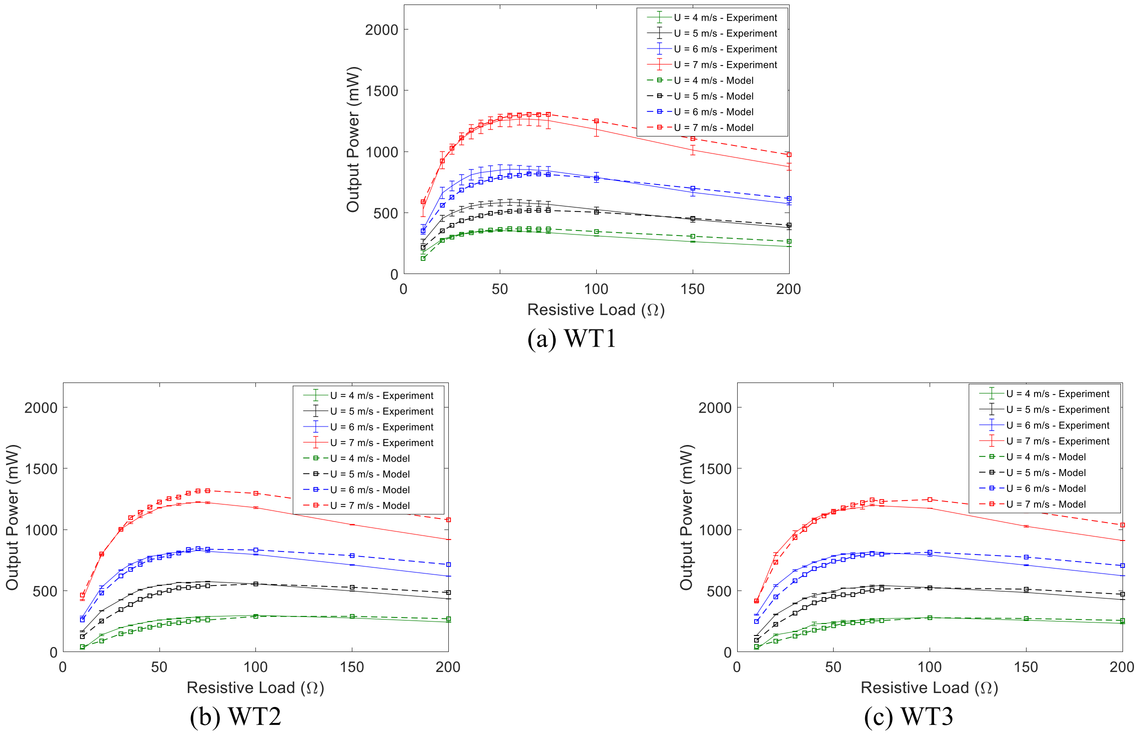


Fig. 8 The output power vs. the load resistance at varying air speeds for different wind turbines: comparison between experimental (solid line) and numerical (dashed line) results

Table 2 Wind turbine inputs/outputs at the maximum power generation

| | Air speed (m/s) | Voltage (V) | Current (mA) | Electrical power (mW) | Wind power (mW) |
|---|---|---|---|---|---|
| WT1 | 4 | 4.201 | 84.74 | 356 | 14,236 |
| | 5 | 5.81 | 101.8 | 591.5 | 27,805 |
| | 6 | 6.671 | 133.53 | 890.8 | 48,047 |
| | 7 | 8.907 | 142.13 | 1266 | 76,297 |
| WT2 | 4 | 5.492 | 54.23 | 297.8 | 6,231 |
| | 5 | 6.351 | 90.21 | 572.9 | 12,156 |
| | 6 | 7.62 | 108.8 | 829.2 | 21,006 |
| | 7 | 9.278 | 132.03 | 1225 | 33,356 |
| WT3 | 4 | 5.302 | 52.88 | 280.4 | 6,231 |
| | 5 | 6.386 | 85.53 | 546.2 | 12,156 |
| | 6 | 7.584 | 108.4 | 821.8 | 21,006 |
| | 7 | 9.145 | 131.34 | 1202 | 33,356 |

good agreement between the experimental and numerical results is obtained. This demonstrates the predictive capability of the electromechanical model. All graphs show a similar trend; that is, an increase in the generated voltage when increasing the load resistance. The rate of the voltage drops as the resistance reaches higher values as can be noticed from the slope of the curves. At a given air speed, the voltage begins saturation when the load resistance reaches 200 Ω. Moreover, at any given electrical load resistance, higher air speeds result in higher voltages generation. We observe that WT2 and WT3 generate the same level of voltage as WT1 under similar operating conditions. The blades of the commercial off-the-shelf wind turbine WT1 have significantly larger size than that of the other wind turbines WT2 and WT3, as shown in Table 1 and then its corresponding available wind power $P_w = \frac{1}{2}\rho A U^3$ is about two times higher than that for WT2 and WT3. This indicates that WT2 and WT3 have better performance. We should mention that WT2 and WT3 have the same size. The only difference is in the pre-twist angle.

We plot in Fig. 8 the output electrical power obtained from the experiments and the electromechanical model as a function of the electrical load resistance for different wind turbines under varying air flow speeds. Again, a good agreement between the two sets of data is observed. The experimental results are also consistent qualitatively with those reported in the literature (Kishore *et al.* 2013, Kishore and Priya 2013, Xu *et al.* 2013, Zakariya *et al.* 2015,

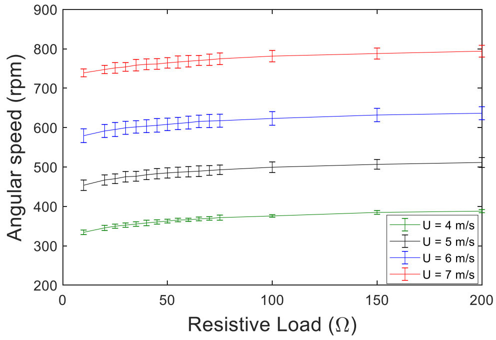


(a) WT1

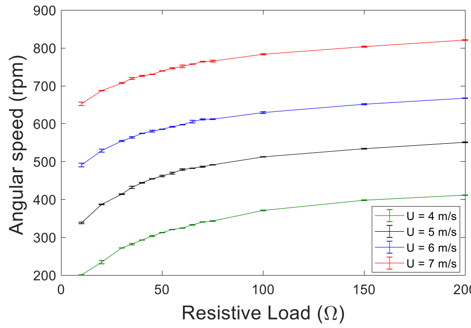


(b) WT2

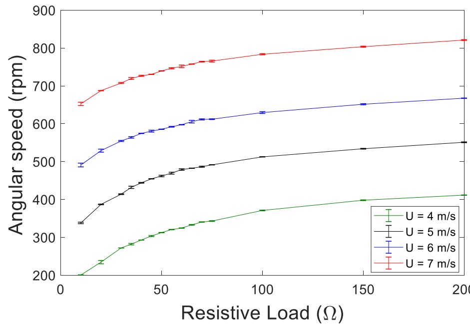


(c) WT3

Fig. 9 Variations of the angular speed of the rotor with the load resistance at varying air speeds for different wind turbines

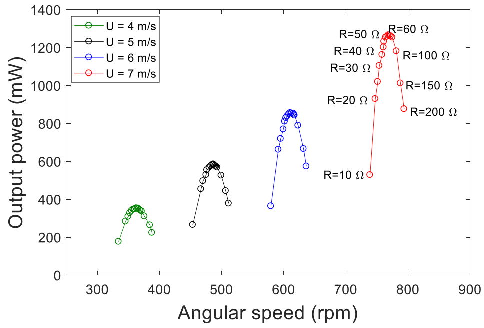


(a) WT1

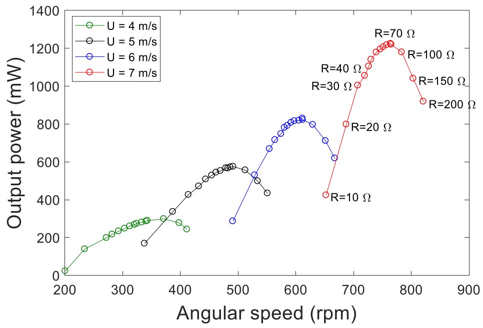


(b) WT2

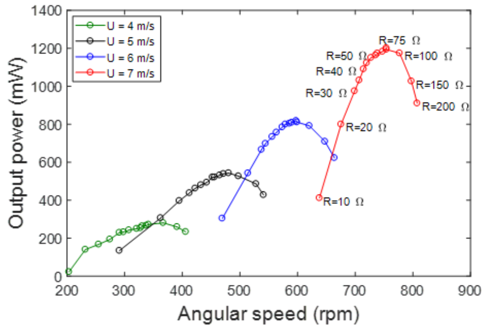


(c) WT3

Fig. 10 Variations of the generated voltage with the angular speed at varying air speeds for different wind turbines (experimental results)

Howey *et al.* 2011, Xu *et al.* 2014, Priya *et al.* 2005). For a given load resistance, increasing the air speed leads to higher power generation. All graphs show the existence of an optimal load resistance leading to a maximum power generation. The optimal resistance increases for higher values of the air speed. This change in the optimal resistance has been observed in previously published experimental studies (Xu *et al.* 2013). In fact, the shift in the optimal resistance is more pronounced for micro-scale wind turbines (rotor diameter < 10 cm). Zakaria *et al.* (2015) performed an experimental investigation of a swirl-type micro-wind turbine. The rotor blade diameter was 2.6 cm. The optimal resistive load was found to decrease from 750 Ω to 320 Ω when increasing the freestream velocity from 3.9 m/s to 8.3 m/s. We note that the opposite trend and the larger variations in the optimal resistive load obtained when increasing the air speed as observed by Zakaria *et al.* (2015) in comparison to the present results are mostly associated to the size of the wind turbine (the rotor diameter is smaller by one order of magnitude), the difference in the level of operational shaft rotational speeds, and the type of the permanent magnet DC motor deployed to produce electricity. For the wind turbine WT1, the maximum generated electrical power when operating at an air speed of 4 m/s is obtained when setting the load resistance equal to 50 Ω. The optimal value of the resistance found equal to 70 Ω for $U$=7 m/s. Kishore and Priya 2013 reported that the optimal resistance ranges from 40 Ω to 60 Ω when operating at an air speed between 2.5 m/s and 5.5 m/s. The electrical power of the wind turbine WT1 reaches a maximum of 1266 mW for the considered range of air speeds. WT2 and WT3 reach their maximum power generation at an optimal load resistance around 100 Ω and 70 Ω at $U$=4 m/s and $U$=7 m/s, respectively. The maximum generated powers obtained for $U$=7 m/s are 1225 mW and 1202 mW for WT2 and WT3, respectively. Table 2 presents the values of the generated voltage, current, and power obtained at the optimal load resistance. These results are showed for different wind turbines and varying air speeds. The corresponding available wind powers are reported as well.

We show in Fig. 9 the angular speed of the wind turbine rotor as function of the load resistance at different air speeds. The results are obtained for the three wind turbines. As expected, increasing the air flow rate speeds up the rotational motion of the blades at a fixed load resistance. The wind turbines run between 200 rpm and 800 rpm for the air speeds ranging from 4 m/s to 7 m/s. The angular speed increases, as the resistance load is increased, and then it stabilizes at constant values, when exceeding large values of the load resistance. A similar trend is obtained for the considered range of the air speeds for all tested wind turbines. This constitutes a typical behavior of a wind turbine, usually referred to as motor reaction of an electric generator (Kishore *et al.* 2013, Kishore and Priya 2013). Low resistance values are observed to lead to higher angular speeds, when deploying WT1 compared to when using WT2 and WT3. Of interest, the measured angular speed of the rotor of WT1 shows less sensitivity to the load resistance when compared to those measured for WT2 and WT3. Higher angular velocities are obtained for WT1 due, in part, to the larger rotor diameter in comparison to the other two turbines. This would result in the generation of a higher mechanical torque when exposed to air flow, which explains the faster rotational motion of WT1. Furthermore, the lower cut-in air speed is observed for WT1, as reported in Table 1, indicates the production of the required torque to initiate the rotational motion at lower air speed. The difference in the angular speed can also be associated with other factors including the twist angle and the blade chord length. The experimental results are in qualitative agreement with those reported in previous experimental research works on small-scale wind turbines (Kishore *et al.* 2013, Kishore and Priya 2013, Xu *et al.* 2013, Zakariya *et al.* 2015, Howey *et al.* 2011, Xu *et al.* 2014, Priya *et al.* 2005).

The plotted curves in Fig. 10 depict the variations of the measured output power with both the angular speed of the wind turbine rotor and the air speed. These experimental results are obtained from wind tunnel tests of the three wind turbines while gradually increasing the load resistance from 10 Ω to 200 Ω. The resistance values are shown as well. Again, we observe the existence of an optimal configuration for each air speed. Clearly, the sensitivity of the electrical power to the load resistance is more significant when operating at higher air speeds. Setting the air speed equal to $U$ = 4 m/s, a 75% increase in the generated power at the optimal load resistance is obtained. Operating at the air speed of $U$ = 7 m/s results in an increase of 136% in the output power for the optimal configuration.

The measured overall efficiency values obtained for varying air speed and loading conditions are shown in Fig. 11. The experimental results reveal that WT1 reaches its maximum overall efficiency at an optimal resistance load of 70 Ω when setting the air speed equal to 4 m/s. The efficiency increases from 1.6% to 2.5% when decreasing the air speed from 7 m/s to 4 m/s. The low efficiency values are mostly associated with the low efficiency of the conversion mechanism from mechanical to electrical power via the gear-generator system as will be shown next. On the other hand, WT2 and WT3 have achieved higher efficiencies in spite of their smaller size in comparison with WT1. WT2 and WT3 reach the maximum efficiency values of 4.8% and 4.5%, respectively, when setting the air speed equal to 4 m/s. The optimal resistance load is found equal to 100 Ω. Unlike the case for WT1, we observe that increasing the air speed from 4 m/s to 5 m/s leads to slight change in the system efficiency.

Next, we use the electromechanical model to estimate the mechanical torque applied on the wind turbine. To do so, we use the Matlab nonlinear curve-fitting tool "*Isqcurvefit*" to identify the numerical values of the torque $T$ and friction coefficient $B$ that lead to the best fit of the experimentally measured electrical power under varying load resistance when using Eq. (16). Fig. 12 shows an example of the nonlinear curve fitting of the electrical power as a function of the load resistance at the wind speed of 5 m/s obtained for the wind turbine WT1. As the Matlab tool "*Isqcurvefit*" is gradient-based optimization method, the choice of the initial guess (starting point) is critical to avoid the algorithm to be trapped in a local optimum. To overcome this issue, we select the initial values of the friction coefficient and the torque using Eqs. 17 and 19, respectively.

Table 3 presents the estimated mechanical torque applied on the wind turbines for different speeds of the airflow. As expected, increasing the air speed leads to

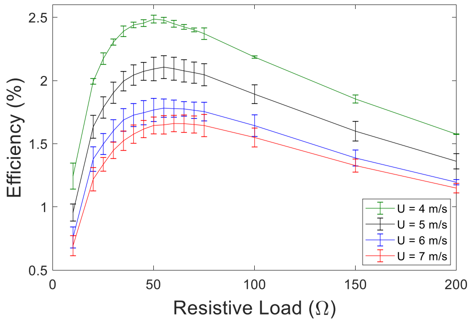


(a) WT1

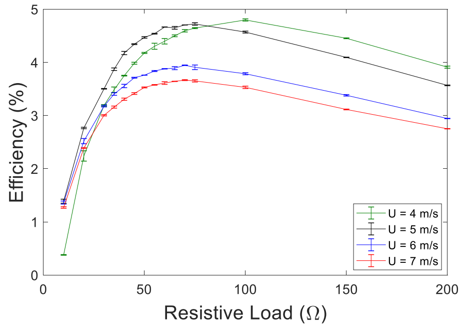


(b) WT2

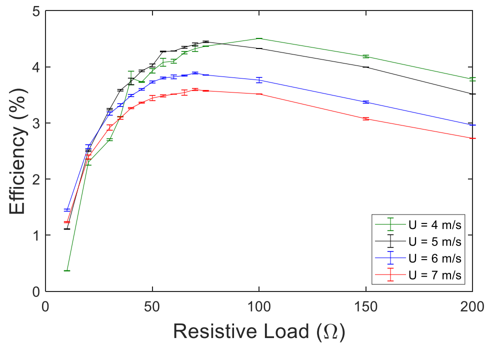


(c) WT3

Fig. 11 Variations of the total efficiency of the rotor with the load resistance at varying air speeds for different wind turbines (experimental results)

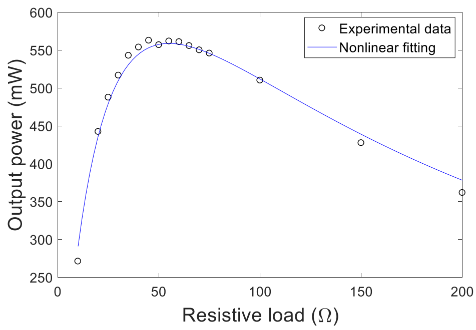


Fig. 12 Electrical power of the wind turbine (WT1) at wind speed of 5 m/s: experimental data and nonlinear fitted data used for mechanical torque estimation

higher driving torques. Given the larger tip diameter of WT1, higher torque values are obtained. We show also in Table 3 the average value of the friction coefficient for each tested wind turbine. The highest value of the friction coefficient is obtained for WT1. This would explain the low performance of the wind turbine WT1 when compared to WT2 and WT3.

Based on the identified torque value, the amount of the mechanical power can be estimated. This estimation leads to the identification of the power coefficient, which represents the amount of mechanical power obtained on the wind turbine rotor shaft for a given wind power. The average values of the estimated power coefficient were 26%, 32% and 30% for the different experiments for wind speeds ranging from 5 to 7 m/s, for the wind turbines WT1, WT2, and WT3, respectively. Therefore, there is a net improvement of the power coefficient for the new designs, despite the reduction in the tip diameter from 68 cm for WT1 to 48 cm for WT2 and WT3. According to the literature (Kishora *et al.* 2013), values of 30% for the power coefficient could be considered as relatively high. It is worth mentioning that the values obtained for the power coefficient for the wind speed of 4 m/s were much lower, which could be explained by the low amount of power harvested at this speed. Indeed, in Table 1, the cut-in speed for the three designs is between 2.3 and 3.8 m/s, which explains the low value of the mechanical torque, hence the low mechanical power, shown in Table 3.

Once the power coefficient is estimated, one can determine the combined efficiency of the gear-generator system. In fact, the measured electrical power and the estimated mechanical power constitute the output and the input of the gear-generator system, respectively. The efficiency of the used gear-generator system is found to have an average value of 6.5% for WT1 and 11.5%, for WT2 and WT3. The increase of the efficiency of the gear-generator system could be explained by the redesign of the shaft mounting for the gears. This fact could also explain the net decrease in the frictional coefficient (Table 3) between the off-the-shelf design, WT1, and the new improved design WT2 and WT3. However, the efficiency is still relatively low and the selection of a new generator is necessary to improve the overall efficiency of the system.

The obtained results show the usefulness of the electromechanical model combined with nonlinear curve fitting to estimate the mechanical torque applied on the

Table 3 Estimated mechanical torque applied on the wind turbine and frictional coefficient

| | Air speed (m/s) | Torque (N-m) | Frictional coefficient (N-ms) |
|---|---|---|---|
| WT1 | 4 | 0.0581 | $4.441\ 10^{-8}$ |
| | 5 | 0.1522 | |
| | 6 | 0.2012 | |
| | 7 | 0.2437 | |
| WT2 | 4 | 0.0187 | $4.598\ 10^{-9}$ |
| | 5 | 0.0868 | |
| | 6 | 0.1045 | |
| | 7 | 0.1269 | |
| WT3 | 4 | 0.0182 | $4.594\ 10^{-9}$ |
| | 5 | 0.0848 | |
| | 6 | 0.1041 | |
| | 7 | 0.1255 | |

wind turbine under varying operating conditions. The power coefficient, expressed as $C_p = \frac{P_{mech}}{(1/2\rho AU^3)} = \frac{T\omega}{(1/2\rho AU^3)}$, is found ranging between 26% and 32%. We recall that $T$ is the torque calculated from the proposed electromechanical model, $\omega$ is the angular speed of the rotor, measured using the laser tachometer, and $U$ is the air speed measured using the anemometer. The obtained values of the power coefficient are quantitatively in agreement with those reported in previously published experimental studies based on small scale wind turbines (Kishora *et al.* 2013, Xu *et al.* 2013). This agreement demonstrates the capability of the proposed model to estimate the mechanical torque. We note that the numerical values of the torque reported in Table 3 can be verified further by deploying a torque sensor mounted on the shaft connecting the rotor of the wind turbine to the gear system. This constitutes our future work that will include the assessment of the mechanical power of the wind turbine and the impact of different system designs on the power coefficient.

## 5. Conclusions

We conducted wind tunnel tests to assess the performance of miniature horizontal axis wind turbines that are expected to be used to provide power supply small sensors and electronic devices in inaccessible or abandoned areas. Three different designs were used in this study. The first one, denoted by WT1, is an off-the-shelf wind turbine and the other two, denoted by WT2 and WT3, constitute our new designs, which were tested to evaluate their performance in terms of electrical power generation. All three wind turbines are equipped with three blades of different geometry, a nacelle box, a rotor, and a gear-generator system (gear ratio 8:1). Several sensors were implemented the wind tunnel to measure the angular speed of the wind turbine rotor, the air speed, the voltage, and the current. A semi-empirical model was developed to estimate the mechanical power on the wind turbine shaft. Using a nonlinear curve-fitting function from MATLAB, the mechanical torque was successfully estimated. From these data, the mechanical power was estimated, which allowed us to evaluate the power coefficient of the blades and the efficiency of the gear-generator system. The obtained results showed a net improvement of the overall efficiency by more than a factor of 2 between WT1 and the new designs WT2 and WT3. The power coefficient, which represents the conversion from the wind energy to the mechanical energy, was increased from 26% for WT1 to 32% for WT2, which is a relatively high value, according to the literature. We note that as per Betz's law, derived from the fundamental principles of mass and momentum conservation on air flow in a disk-shaped actuator, the maximum power that a turbine can capture is 59.3% of the kinetic energy of the wind (M. Ragheb and A. M. Ragheb 2011). This does not account for losses due to other components such as the gearbox, the rotor shaft, the electric generator, and the bearings. Thus, wind turbines cannot reach Betz limit, especially the small ones, which are subject to higher viscous drag, friction and thermal losses. Finally, the gear-generator efficiency was found to be relatively low, despite its improvement from 6.5% for WT1 to 11.5% for WT2 and WT3. In conclusion, the proposed design is acceptable from an aerodynamic perspective given its capability in terms of mechanical power extraction from the available wind energy, however, the gear-generator system needs more careful selection.

## Acknowledgements

The study presented in the paper was financially supported via the faculty research grants (FRG17-R-030 and EN6001) from the American University of Sharjah.

## Conflict of Interest

The authors declare that they have no conflict of interest.

## References

Bukala, J., Damaziak, K., Karimi, H.R. and Malachowski, J. (2016), "Aero-elastic coupled numerical analysis of small wind turbine - generator modelling", *Wind Struct*., **23**(6), 577-594. https://doi.org/10.12989/was.2016.23.6.577.

Carta, J.A., Gonzalez, J., Cabrera, P. and Subiela, V.J. (2015), "Preliminary experimental analysis of a small-scale prototype SWRO desalination plant, designed for continuous adjustment of its energy consumption to the widely varying power generated by a stand-alone wind turbine", *Appl. Energy*, **137**, 222-239. https://doi.org/10.1016/j.apenergy.2014.09.093.

Castagnetti, D. and Radi, E. (2018), "A piezoelectric based energy harvester with dynamic magnification: modelling, design and experimental assessment", *Meccanica*, **53**(11-12), 2725-2742.

Costa Rocha, P.A., Carneiro de Aroujo, J.W., Pontes Lima, R.J., Vieira da Silva, M.E., de Andrade, C.F. and Carneiro, F.O.M. (2018), "The effects of blade pitch angle on the performance of small-scale wind turbine in urban environments", *Energy*, **148**, 169-178. https://doi.org/10.1016/j.energy.2018.01.096.

De Broe, Drouilhet A.M. and Gevorgian, V. (1999), "A peak power tracker for small wind turbines in battery charging applications", *IEEE T. Energy Conver.*, **14**(4), 1630-1635. https://doi.org/10.1109/60.815116.

Du, B., Cuala, M., Lei, L. and Zeng P. (2019), "Experimental investigation of the performance and wake effect of a small-scale wind turbine in a wind tunnel", *Energy*, **166**, 819-833. https://doi.org/10.1016/j.energy.2018.10.103.

Erturk, A. and Inman D.J. (2011), Piezoelectric Energy Harvesting, John Wiley and Sons. United Kingdom.

Hirahara, H., Hossain, M.Z., Kawahashi, M. and Nonomura, Y. (2005), "Testing basic performance of a very small wind turbine designed for multi-purposes', *Renew. Energy*, **30**(8), 1279-1297. https://doi.org/10.1016/j.renene.2004.10.009.

Howey, D., Bansal, A. and Holmes, A. (2011), "Design and performance of a centimeter-scale shrouded wind turbine for energy harvesting", *Smart Mater. Struct.*, **20**(8), 085021. https://doi.org/10.1088/0964-1726/20/8/085021.

Kishore, R.A., Courdron, T. and Priya, S. (2013), "Small-scale wind energy portable turbine (SWEPT)", *J. Wind Eng. Ind. Aerod.*, **116**, 21-31. https://doi.org/10.1016/j.jweia.2013.01.010.

Kishore, R.A. and Priya, S. (2013), "Design and experimental verification of a high efficiency small wind energy portable turbine (SWEPT)", *J. Wind Eng. Ind. Aerod.*, **118**, 12-19. https://doi.org/10.1016/j.jweia.2013.04.009.

Morshed, K.N., Rahman, M., Molina, G. and Ahmed, M. (2013), "Wind tunnel testing and numerical simulation on aerodynamic performance of a three-bladed Savonius wind turbine", *Int. J. Energy Environ. Eng.*, **4**(1), 4-18. https://doi.org/10.1186/2251-6832-4-18.

Ottman, G.K., Hofman, H.F., Bhatt, A.C. and Lesieutre, G.A. (2002), "Adaptive piezoelectric energy harvesting circuit for wireless remote power supply", *IEEE T. Power Electr.*, **17**(5), 669-676. https://doi.org/10.1109/TPEL.2002.802194.

Park, J.W., Jung, H.J., Jo, H. and Spencer, B.F. (2012), "Feasibility study of micro-wind turbines for powering wireless sensors on a cable-stayed bridge", *Energies*, **5**, 3450-3464. https://doi.org/10.3390/en5093450.

Perez, M., Boisseau, S., Gasnier, P., Willemin, J., Geisler, M. and Reboud, J.L. (2016), "A cm scale electret-based electrostatic wind turbine for low-speed energy harvesting applications", *Smart Mater. Struct.*, **25**(4), 045015. https://doi.org/10.1088/0964-1726/25/4/045015.

Priya, S., Chen, C.T., Fye, D. and Zahnd, J. (2005), "Piezoelectric windmill: A novel solution to remote sensing", *Jpn. J. Appl. Phys.*, **44**(3), 104-107. https://doi.org/10.1143/JJAP.44.L104.

Ragheb, M. and Ragheb, M.A. (2011), "Wind turbines theory - the betz equation and optimal rotor tip speed ratio, *Fundamental Advan. Top. Wind Power*", **1**(1), 19-38.

Roy, S. and Saha, U.K. (2015), "Wind tunnel experiments of a newly developed two-bladed Savonius-style wind turbine", *Appl. Energy*, **137**, 117-125. https://doi.org/10.1016/j.apenergy.2014.10.022.

ScienceKit (2018), Wind Power V3: Renewable Energy Science Kit; Thames and Cosmos, USA https://www.thamesandkosmos.com/index.php/8-to-10/wind power-v3.

Shah, H., Mathew, S. and Lim C.M. (2014), "A novel low reynolds number airfoil design for small horizontal axis wind turbines", *Wind Eng.*, **38**(4), 377-391. https://doi.org/10.1260%2F0309-524X.38.4.377.

Sodano, H.A., Inman, D.J. and Park, G. (2005), "Comparison of piezoelectric energy harvesting devices for recharging batteries", *J. Intel. Mater. Sys. Struct.*, **16**(10), 799-807. https://doi.org/10.1177/1045389X05056681.

Syta, A., Bowen, C.R., Rysak, A. and Litak, G. (2015), "Experimental analysis of the dynamical response of energy harvesting devices based on bistable laminated plates", *Meccanica*, **50**(8), 1961-1970. https://doi.org/10.1007/s11012-015-0140-1.

Tarhan, C. and Yilmaz, I. (2019), "Numerical and experimental investigations of 14 different small wind turbine airfoils for 3 different Reynolds number conditions", *Wind Struct.*, **28**(3), 144-153. https://doi.org/10.12989/was.2019.28.3.141.

Xu, F., Yuan, F.G., Liu, L., Hu, J. and Qiu, Y. (2013), "Performance prediction and demonstration of a miniature horizontal axis wind turbine", *J. Energy Eng.*, **139**(3), 143-152. https://doi.org/10.1061/(ASCE)EY.1943-7897.0000125.

Xu, F.J., Yuan, F.G., Hu, J.Z. and Qiu, Y.P. (2014), "Miniature horizontal axis wind turbine system for multipurpose application", *Energy*, **75**, 216-224. https://doi.org/10.1016/j.energy.2014.07.046.

Zakariya, M., Pereira, D.A. and Hajj, M.R. (2015), "Experimental investigation and performance modeling of centimeter-scale micro-wind turbine energy harvesters", *J. Wind Eng. Ind. Aerod.*, **147**, 58-65. https://doi.org/10.1016/j.jweia.2015.09.009.

Zhou, M., Fu, Y., Xu, Z., Al-Furjan, M.S. and Wang, W. (2018), "Modeling and preliminary analysis of piezoelectric energy harvester based on cylindrical tube conveying fluctuating fluid", *Meccanica*, **53**(9), 2379-2392.

*CC*